2019 IEEE 16th International Symposium on Biomedical Imaging (ISBI 2019)
Venice, Italy, April 8-11, 2019

# DMR-CNN: A CNN TAILORED FOR DMR SCANS WITH APPLICATIONS TO PD CLASSIFICATION

*Monami Banerjee*[1†], *Rudrasis Chakraborty*[2†], *Derek Archer*[1], *David Vaillancourt*[1] *and Baba C. Vemuri*[1]

[1] University of Florida, Gainesville, FL, USA
[2] University of California, Berkeley/ ICSI

† Equal contribution

## ABSTRACT

Convolutional neural networks are ubiquitous in Machine Learning applications for solving a variety of problems. They however can not be used in their native form when the domain of the data is commonly encountered manifolds such as the sphere, the special orthogonal group, the Grassmannian, the manifold of symmetric positive definite matrices and others. Most recently, generalization of CNNs to Riemannian homogeneous spaces have been reported in literature. In this work, we propose an end-to-end CNN architecture for classification of diffusion MRI (dMRI) signals, dubbed dMR-CNN. In each voxel of the dMRI scan, the signal is acquired as a real number along each diffusion sensitizing magnetic field direction over a hemi- sphere of directions in 3D. Hence, in each voxel, we have a function $f : \mathbf{S}^2 \times P_1 \to \mathbf{R}$. We formulate a definition of correlation on this space to extract *intra*-voxel features and then use standard CNN model to capture the spatial interactions between the *intra*-voxel features. Our proposed framework comprises of architectures to extract these *intra*- and *inter*- voxel features. We present an experimental setup to classify dMRI scans acquired from a cohort of 44 Parkinson Disease patients and 50 control/normal subjects.

***Index Terms***— dMR-CNN, Equivariance

## 1. INTRODUCTION

CNNs introduced in [1] have gained enormous attention in the past decade especially after the demonstration of the significant success on Imagenet data by [2] and others. The key property of equivariance to translation of patterns in the image is utilized in the CNN to share learned weights across a layer in the network. Thus, one might consider exploiting equivariance to transformation groups as a key design principle in designing neural network architectures suitable for these groups. For data sets that are samples of functions defined on Riemannian manifolds, it would then be natural to seek a symmetry group action that the manifold naturally admits and define the correlation operation (on the manifold) that would be equivariant to this symmetry group action. Several researchers [3, 4] proposed convolutional/correlational models which are equivariant to the action of the symmetry group admitted by the sphere in 3D. Recently in [5, 6], the authors proposed a definition of correlation on a Riemannian homogeneous space [7] which is symmetry group equivariant.

In this work, we present a novel architecture for implementing the CNN suited for Riemannian homogeneous spaces (called HCNN for homogeneous CNN) of which the domain of the dMRI data is an example. Our overall network called dMR-CNN is a combination of HCNN that captures intra-voxel features and a standard CNN that captures inter-voxel interactions of these intra-voxel features. We include experiments depicting, to the best of our knowledge, for the first time an end-to-end implementation for classification of diffusion MRI (dMRI) brain scans of Parkinson Disease (PD) patients and control subjects. Our formulation involves defining correlation operation on the Riemannian homogeneous space $\mathbf{S}^2 \times P_1$ (where $P_1$ is the space of positive reals). The experiment involves classification of dMRI scans acquired from a cohort of 44 PD patients and 50 Controls. We present an end-to-end classification of dMRI brain scans. dMRI is a non-invasive magnetic resonance imaging technique that allows for inference of neuronal connectivity between various neuroanatomical structures using a diffusion sensitized MR signal [8]. Typically, diffusion sensitizing magnetic field gradients are applied along a large number of directions and the response MR signal is collected at each voxel along these directions. For each direction, the data contains an entire MR volume image. Let $S(\mathbf{q})$, denote the scalar valued signal at a voxel in the 3D image along a radial vector $\mathbf{q}$ in the Fourier (frequency) space. Since $\mathbf{q}$ is a radial vector with a magnitude and a direction, the natural mathematical space for representing this signal $S(\mathbf{q})$ is then by functions on the product space, $\mathbf{S}^2 \times P_1$. This product space is a Riemannian homogeneous space. Using the spherical harmonic basis on $\mathbf{S}^2$ – which form a basis for all $L^2$ functions on the sphere – along with Laguerre polynomials for representing the radial part, we present a symmetry group equivariant correlation

THIS RESEARCH WAS FUNDED IN PART BY THE NSF GRANT IIS-1525431 AND IIS-1724174 TO BCV

for such functions. The product is known as the SHORE basis in dMRI literature [9, 10]. In the following sections, we will present the theory and implementation along with experiments for this setting.

## 2. CORRELATION ON RIEMANNIAN HOMOGENEOUS SPACES

In this section, we first briefly give an overview on the differential geometry of the Riemannian homogeneous space $\mathbf{S}^2 \times P_1$ which is required to define the correlation operation, where $P_1$ is the space of positive reals. For a detailed exposition on the geometry of the Riemannian homogeneous spaces, we refer the reader to a comprehensive and excellent treatise by Helgason [7].

**Preliminaries.** Let $(\mathcal{M}, g^{\mathcal{M}})$ be a Riemannian manifold with a Riemannian metric $g^{\mathcal{M}}$, i.e., $(\forall x \in \mathcal{M})\ g_x^{\mathcal{M}} : T_x\mathcal{M} \times T_x\mathcal{M} \to \mathbf{R}$ is a bi-linear symmetric positive definite map, where $T_x\mathcal{M}$ is the tangent space of $\mathcal{M}$ at $x \in \mathcal{M}$. Let $d : \mathcal{M} \times \mathcal{M} \to \mathbf{R}$ be the metric (distance) induced by the Riemannian metric $g^{\mathcal{M}}$. Let $I(\mathcal{M})$ be the set of all isometries of $\mathcal{M}$, i.e., given $g \in I(\mathcal{M})$, $d(g.x, g.y) = d(x, y)$, for all $x, y \in \mathcal{M}$. It is clear that $I(\mathcal{M})$ forms a group (henceforth, we will denote $I(\mathcal{M})$ by $G$) and thus, for a given $g \in G$ and $x \in \mathcal{M}$, $g.x \mapsto y$, for some $y \in \mathcal{M}$ is a group action. Since we choose the left group action, we will denote it by $L_g$, i.e., $L_g(x) = g.x$. *Note that $L_g : \mathcal{M} \to \mathcal{M}$ is a diffeomorphism.* Consider $o \in \mathcal{M}$, and let $H = \text{Stab}(o) = \{h \in G | h.o = o\}$, i.e., $H$ is the *Stabilizer* [11] of $o \in \mathcal{M}$. We say that $G$ acts *transitively* on $\mathcal{M}$, *iff*, given $x, y \in \mathcal{M}$, there exists a $g \in \mathcal{M}$ such that $y = g.x$. For $\mathcal{M} = \mathbf{S}^2 \times P_1$, $G = \mathsf{SO}(3) \times \{\mathbf{R} \setminus \{0\}\}$ and $H = \mathsf{SO}(2) \times \{\pm 1\}$. For the notational simplicity, throughout the rest of the paper, we will use $\mathcal{M}$ to denote $\mathbf{S}^2 \times P_1$ and $G$ and $H$ to denote the respective group and the stabilizer.

In fact, one can identify $\mathcal{M}$ as a Riemannian homogeneous space [7] and hence, the following identities are true. 1. $d(x, z) = d(g.z, g.z)$ 2. $\int_{\mathcal{M}} f(y)\omega(x) = \int_{\mathcal{M}} f(x)\omega(x)$ , where, $f : \mathcal{M} \to \mathbf{R}$ is any integrable function with respect to the volume density $\omega$ corresponding to the Riemannian metric $g^{\mathcal{M}}$, $x, y, z \in \mathcal{M}$ and $g \in G$. Now, we will present some definitions needed to define the correlation operator.

**Definition 2.1 (Pullback of a function $f$ using the diffeomorphism $L_{g^{-1}}$).** *Let $f : \mathcal{M} \to \mathbf{R}$ be a function on $\mathcal{M}$. We can define the pullback of $f$ by the diffeomorphism $L_{g^{-1}}$ denoted by $\left(L_{g^{-1}}\right)^* f : \mathcal{M} \to \mathbf{R}$ as $y \mapsto f\left(L_{g^{-1}}(y)\right)$.*

For the rest of the paper we will assume a function $f : \mathcal{M} \to \mathbf{R}$ to be square integrable, i.e., $|f(x)|^2 \omega^{\mathcal{M}}(x) < \infty$, if not mentioned otherwise.

Now, we will define correlation of two functions on the Riemannian homogeneous space $\mathcal{M}$.

**Definition 2.2 (Correlation).** *Using the above notations, the correlation between $f$ and $w$ is given by, $(f \star w) : G \to \mathbf{R}$ defined as follows:*

$$(f \star w)(g) := \int_{\mathcal{M}} f(x) \left(L_{g^{-1}}^* w\right)(x) \omega^{\mathcal{M}}(x) \qquad (1)$$

Let $S = \{f : \mathcal{M} \to \mathbf{R}\}$ and $U = \{(f \star w) : G \to \mathbf{R} | f \in S\}$. Then, the following proposition holds with the proof presented in [6].

**Proposition 2.1.** *Let $F : S \to U$ be a function given by $f \mapsto (f \star w)$. Then, $F$ is $G$-equivariant [6].*

We now propose an convolutional architecture to classify the dMRI data.

### 2.1. Network architecture

In each voxel of the dMRI scan, the signal is acquired as a real number along each magnetic field direction over a hemisphere of directions in 3D. Hence, in each voxel, we have a function $f : \mathbf{S}^2 \times \mathbf{R}^+ \to \mathbf{R}$. As described earlier, we will use the well known SHORE basis [9] to represent each function. Our proposed network architecture has two components, to extract *intra-voxel features* and *inter-voxel features* respectively. Below, we will describe both of these layers separately. A figure depicting the network architecture for dMRI classification is included in Fig. 1.

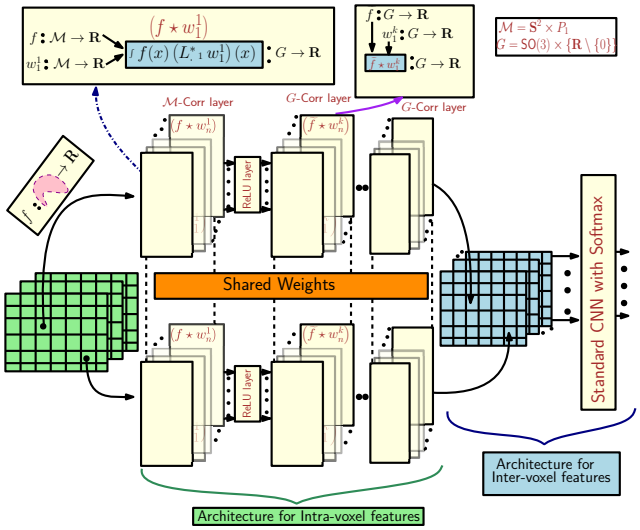


**Fig. 1**: Schematic diagram of dMR-CNN

#### 2.1.1. Extracting intra-voxel features

In order to extract intra-voxel features, we will treat each voxel independently. As mentioned before, in each voxel we have a function $f : \mathbf{S}^2 \times \mathbf{R}^+ \to \mathbf{R}$. Since $\mathbf{S}^2 \times \mathbf{R}^+$ is a Riemannian homogeneous space (endowed with the product

metric), we will use a sequence of correlation layers (with non-linearity within) to extract features which are *equivariant* to the action of $\mathsf{SO}(3) \times (\mathbf{R} \setminus \{0\})$. The architecture to extract this intra-voxel features consists of three layers described below. For simplicity of notations, we will use $\mathcal{N}$ to denote $\mathbf{S}^2 \times \mathbf{R}^+$ and $G$ to denote $\mathsf{SO}(3) \times (\mathbf{R} \setminus \{0\})$.

**Correlation on $\mathcal{M}$ ($\mathcal{M}$-Corr)**: Let $f \in L^2(\mathcal{M}, \mathbf{R})$ be the input function and $w \in L^2(\mathcal{M}, \mathbf{R})$ be the mask. Then, using definition 2.2, $\mathcal{M}$-Corr is defined as $(f \star w) : G \to \mathbf{R}$.

**Correlation on $G$ ($G$-Corr)**: Let $\widetilde{f} \in L^2(G, \mathbf{R})$ be the input function and $w \in L^2(G, \mathbf{R})$ be the mask. Then analogous to $\mathcal{M}$-Corr, we can define $G$-Corr as $\left(\widetilde{f} \star w\right) : G \to \mathbf{R}$ using definition 2.2 (as $G$ naturally acts on $G$).

In order to use nonlinearity between two layers, we will add a ReLU unit. As the outputs of both $\mathcal{M}$-Corr and $G$-Corr are functions from $G$ to $\mathbf{R}$, we will use the standard ReLU operation on $\mathbf{R}$.

We will use a cascade of these layers to extract the features – from each voxel independently – that are equivariant to the action of $G$. Observe that this equivariance property is natural in the context of dMRI data. Since in each voxel of the dMRI data, the signal is accquired in different directions (in 3D), we want the features to be equivariant to the 3D rotations and scaling (given by $G = \mathsf{SO}(3) \times \{\mathbf{R} \setminus \{0\}\}$). Thus, our formulation extracts features which are natural to the dMRI data.

### *2.1.2. Extracting inter-voxel features*

After the extraction of the intra-voxel features (which are equivariant to the action of $G$), we want to derive features based on the interactions between the neighboring voxels. We will use a cascade of standard convolutional and ReLU layers to capture the interaction between the equivariant intra-voxel features. This process yields features capturing the interactions between intra-voxel features over a spatial neighborhood. One can of course treat the intra-voxel features as a bag of features and use a fully connected layer. But, we will show using permutation testing in Section 3 that capturing interaction between features across voxels gives statistically significant results, while without this layer the result is not statistically significant. We provide the details about this statistical testing in the experimental section. We will call this network architecture dMR-CNN.

## 3. EXPERIMENTS

In this section, we present a real data experiment that involves classification of dMRI brain scans acquired from a cohort of Parkinson Disease (PD) patients and control subjects.

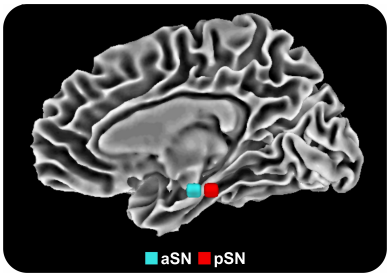


**Fig. 2**: A sample $S(\mathbf{0})$ image with overlayed ROIs

For the dMRI data, we used the raw signal, $S(\mathbf{q})$ at each voxel as our input data. The data pool consists of dMRI (human) brain scans acquired from 50 PD patients and 44 controls. All images were collected using a 3.0 T MR scanner (Philips Achieva) and 32-channel quadrature volume head coil. The parameters of the diffusion imaging acquisition sequence were as follows: gradient directions = 64, b-values = 0/1000 s/mm2, repetition time =7748 ms, echo time = 86 ms, flip angle = $90^\circ$, field of view = $224 \times 224$ mm, matrix size = $112 \times 112$, number of contiguous axial slices = 60, slice thickness = 2 mm, and SENSE factor P = 2.

From each subject, the left/right anterior and posterior substantia nigra (aSN and pSN respectively) were manually segmented by an expert. We restrict our attention to these 4 regions-of-interest (ROIs) for the classification task as they are known to be affected most by PD. Eddy current correction was applied to each data set by using standard motion correction techniques. Fig. 2 depicts an example of $S_0$ (zero magnetic gradient) image in the MNI standard coordinate space overlayed with two of the ROIs.

Below, we provide the details of our classification experiment. We selected 85 subjects at random to train on and the remaining 9 were used for testing.

**Classification of dMRI data:** For each ROI, we extracted the intra-voxel features using the HCNN with weights shared across voxels in the same ROI. The network architecture to extract intra-voxel features is as follows $\mathcal{M}$-Corr $\to$ ReLU $\to$ $G$-Corr $\to$ ReLU $\to$ $G$-Corr with the number of channels being 5, 10 and 15 respectively. Furthermore, we use batch-normalization after each convolution layer. Then, for each ROI, we extracted inter-voxel features using two $2 \times 2$ convolution layers with number of channels 20 and 25 respectively. We used $2 \times 2$ standard batch-normalization, max-pool and ReLU in between.

After, extracting inter voxel features, we combined features from 4 ROIs using a log-softmax fully connected layer with negative log-likelihood loss at the end. We used the stochastic gradient decent (SGD) as the optimizer with an initial step size of 0.1 and a step decay learning rate update. The total number of parameters for this network is 32482. We trained this model for 94 epochs and obtained 95.24% training and 88.88% testing accuracy. The total training time is 9328.8 seconds. The above testing accuracy implies misclassification of one test sample.

**Permutation testing for statistical significance of inter-voxel features:** Now, we present a Hotelling $T^2$ statistic and use this test to assess the statistical significance of group differences. In order to achieve this, we perform a permutation test. Since it is difficult to formulate a parametric permutation test for this data, we use a non-parametric permutation test instead. The steps involved in performing the permutation test are as follows: (i) compute the $t^2$ statistic. (2) randomly permute the data between PD and control groups, and then compute $t_i^2$. (3) Repeat step (2) $50,000$ times and report the p-value as the fraction of times $t_i^2 > t^2$. The resultant p-value can be interpreted as the probability of finding a larger group difference by randomly permuting the data. We will reject the null hypothesis that there is no difference between the group means with $5\%$ significance. The p-values for both dMR signal and EAP-based representations for inter- and intra-voxel features are reported in Table 1. We computed the p-values for each ROI independently.

| Mode | Intra/ Inter | ROI aSN (L) | aSN (R) | pSN (L) | pSN (R) |
|---|---|---|---|---|---|
| dMR | Intra | 0.39 | 0.52 | 0.45 | 0.97 |
| dMR | Inter | **0.00** | **0.00** | **0.00** | **0.00** |

**Table 1**: p-values for permutation testing.

In the above table, aSN/pSN (L/R) represent the left/right anterior/posterior substantia nigra respectively. By examining the p-values in Table 1, we can see that intra-voxel features are not statistically significant in finding the group difference, while after examining the interaction between equivariant features, we can reject the null hypothesis. This justifies the need for inter-voxel feature layer. Furthermore, we used a fully connected layer after extracting intra-voxel features and obtained around $50\%$ classification accuracy (i.e., uniform class probabilities). This in conjunction with the hypothesis testing described above indicates the usefulness of inter-voxel features. But, one may wonder about the usefulness of intra-voxel features, hence we applied a 3D CNN to the dMR signal and obtained a classification accuracy of $66.67\%$. This clearly justifies the need and importance of both inter- and intra-voxel layers. Furthermore, the results in Table 1 indicate that, using the dMR raw signal representation, features extracted from all the $4$ ROIs are statistically significant.

## 4. CONCLUSIONS

In this paper, we presented a novel deep network architecture called dMR-CNN, which is a cascade of two types of architectures, (i) a novel generalization of the CNN to cope with data whose domain is a Riemannian homogeneous space abbreviated HCNN. This architecture extracts the intra-voxel features. (ii) a standard CNN, which captures the inter-voxel neighborhood interactions between the intra-voxel features. We presented the an end-to-end deep network architecture for classification of dMRI brain scans acquired from a cohort of 44 Parkinson Disease patients and 50 controls. Statistical group testing results were presented depicting the significance of the classification results. Our future work will focus on testing on dMRI brains scans from a larger populations of PD patients and control subjects.

## 5. REFERENCES


[1] Yann LeCun, Léon Bottou, Yoshua Bengio, and Patrick Haffner, "Gradient-based learning applied to document recognition," *Proceedings of the IEEE*, vol. 86, no. 11, pp. 2278–2324, 1998.

[2] Alex Krizhevsky and Geoffrey Hinton, "Learning multiple layers of features from tiny images," Tech. Rep., Tech. Report, University of Toronto, 2009.

[3] T.S. Cohen, M. Geiger, J. Koehler, and M. Welling, "Spherical CNNs," in *Proceedings of ICLR*. 2018, JMLR.

[4] Carlos Esteves, Christine Allen-Blanchette, Xiaowei Zhou, and Kostas Daniilidis, "Polar transformer networks," *arXiv preprint arXiv:1709.01889*, 2017.

[5] Risi Kondor and Shubhendu Trivedi, "On the generalization of equivariance and convolution in neural networks to the action of compact groups," *arXiv preprint arXiv:1802.03690*, 2018.

[6] Rudrasis Chakraborty, Monami Banerjee, and Baba C Vemuri, "H-cnns: Convolutional neural networks for riemannian homogeneous spaces," *arXiv preprint arXiv:1805.05487*, 2018.

[7] Sigurdur Helgason, *Differential geometry and symmetric spaces*, vol. 12, Academic press, 1962.

[8] Peter J Basser, James Mattiello, and Denis LeBihan, "Mr diffusion tensor spectroscopy and imaging," *Biophysical journal*, vol. 66, no. 1, pp. 259–267, 1994.

[9] Evren Özarslan, Cheng Guan Koay, Timothy M Shepherd, Michal E Komlosh, M Okan İrfanoğlu, Carlo Pierpaoli, and Peter J Basser, "Mean apparent propagator (MAP) MRI: a novel diffusion imaging method for mapping tissue microstructure," *NeuroImage*, vol. 78, pp. 16–32, 2013.

[10] Rutger HJ Fick, Demian Wassermann, Emmanuel Caruyer, and Rachid Deriche, "MAPL: Tissue microstructure estimation using laplacian-regularized MAP-MRI and its application to hcp data," *NeuroImage*, vol. 134, pp. 365–385, 2016.

[11] David Steven Dummit and Richard M Foote, *Abstract algebra*, vol. 3, Wiley Hoboken, 2004.